Time Domain Traveling Wave analysis of the multimode dynamics of Quantum Dot Fabry-Perot Lasers

Time Domain Traveling Wave analysis of the multimode dynamics of Quantum Dot Fabry-Perot Lasers

Mariangela Gioannini, Paolo Bardella and Ivo Montrosset, *Member, IEEE*

***Abstract*—In this paper we investigate with numerical simulations the rich multi-mode dynamics of Quantum Dot Fabry-Perot Lasers. We have used a Time Domain Traveling Wave approach including the electron and hole carrier dynamics in the various Quantum Dot confined states, the inhomogeneous broadening of the complex gain spectrum, the polarization dynamics and the effect of the carrier-photon interaction in the cavity. The role of the various non-linear interaction mechanism on the broadening of optical spectrum of the Quantum Dot laser has been investigated and the main parameters responsible for the phase locking between the longitudinal modes have been identified. We show that in some cases it is possible obtaining pulses after simulating the propagation of the laser output field in a dispersive medium. Many of the obtained simulation results are in good agreement with the experiments reported in the literature.**

***Index Terms*—Quantum Dot semiconductor lasers, Fabry-Perot lasers, Time Domain Traveling Wave simulations, Multimode dynamics, mode locking.**

I. Introduction

THE complicate dynamics of multi-mode Fabry-Perot (FP) Semiconductor Laser and the various physical effects at the origin of the multi-mode coupling have been investigated from long time in various materials systems: bulk lasers were considered for example in [1]–[7], Quantum Well (QW) lasers in [8]–[10] and Quantum Cascade (QC) lasers in [11], [12].

Recently, several experimental works on Quantum Dash (QDash) [13], [14] and Quantum Dot (QD) [15]–[18] lasers have shown the possibility of generating wide optical comb spectra with a single section FP cavity and, frequently, the emission of a pulse train directly at the laser output [15] or after propagation in a proper length of dispersive optical fiber [13], [17]. This phase locking regime obtained in a single section FP laser will be indicated hereafter as self-mode locking (SML) regime, to distinguish it from the passive-mode locking (PML) regime where a saturable absorber section is required.

In the last years the research on SML at the optical communication wavelengths has almost focused on the QDash and QD material systems, but it is important to point out that SML is not peculiar of nano-structured active materials since it was reported also for QWell lasers in a few papers [9], [10]. Compared to the QW counterpart, the QDash lasers have provided higher output power, broader optical spectrum and smaller linewidth of the RF line at the cavity round trip frequency [19]. The SML mechanism seems also more robust in nano-structure materials since it has been found by several independent groups on different FP samples and, recently, also in QD based VCSELs [20]. QDash and QDs seem therefore more promising for this application because, thanks to the inhomogeneous broadening of the gain spectrum, a wide optical spectrum of lasing modes above threshold can be achieved [21]. It is important to note that the broad optical spectrum often measured in QD and QDash lasers does not automatically imply that a phase-locking condition can be established among all the modes; in [14] for example the phase locking is achieved only within separate clusters of modes indicated as super-modes.

All these interesting results and the many possible applications of these simple lasers in several optical systems have stimulated the research towards the understanding of the non-linear mechanism that makes the longitudinal modes running as synchronized oscillators. Many are the physical effects cited in the literature for explaining SML in QD and QDash lasers; these are the Four Wave Mixing (FWM) [22], the Kerr effect together with Self and Cross Phase Modulation [15] and the Two-Photon Absorption (TPA) [18]. Similarly to the QD laser case, the QC lasers have also demonstrated the possibility of a multi-longitudinal mode regime with broad optical spectrum and narrow RF beat note at the cavity round-trip frequency [11]. In [11] this behavior is attributed to the strong Fast varying Longitudinal Spatial Hole Burning (Fast-LSHB) that causes longitudinal carrier gratings with period one-half of the wavelength originated by the field standing wave pattern in the FP cavity. These gratings are responsible for the coupling among the modes. The authors of [11] demonstrate that this strong Fast-LSHB is possible because the gain recovery dynamics in the QC is much faster than the carrier diffusion process. A second mechanism also considered in [11] is the Kerr effect; this one was included as an instantaneous saturable absorber distributed all over the device length. We however point out that the results in [11] show that Kerr effect plays a secondary role respect to the Fast-LSHB; this LSHB is indeed responsible for the broadening of the optical spectrum whereas Kerr effect gives a more pronounced splitting of the optical spectrum in two or more clusters of modes.

The QD material system seems therefore more similar to the QC case rather than the QW case. In QDs indeed the Fast-LSHB of the carriers in the lasing ground state cannot be

Authors are with the Dipartimento di Elettronica e Telecomunicazioni, Politecnico di Torino, Corso Duca degli Abruzzi 24, 10129 Torino, Italy email: mariangela.gioannini@polito.it

Manuscript received xxx, 2015; revised YYY, 2015.

washed out by diffusion because carrier diffusion cannot occur in a 0D states [23], [24]. Theoretical works have demonstrated that the carrier gratings originated by the standing wave pattern cause a saturation of the gain at the lasing mode wavelength and this saturation can be modeled as a gain compression factor parameter (also known as ε parameter) [25], [26] [27]. Several experimental works have also reported measurements or evidences of high ε-parameter as a peculiar characteristic of the QD lasers [28]–[30], [31].

The role of the carrier gratings due to Fast-LSHB and of the carrier diffusion in the broadening the QW FP optical spectrum was studied using a Traveling Wave model already in [5]: the numerical simulations evidenced that without Fast-LSHB the FP spectrum is always single mode even well above threshold. On the contrary, if the Fast-LSHB is included and the diffusion is set to zero, the FP optical spectrum broadens with current. However in [5] no spectral hole burning effect was included in the model. After [5], the simulation of the coupled dynamics of the longitudinal modes in bulk and QW FP lasers has been undertaken in several other works such as [8], [32]. In [8] and [32] the authors assumed that the longitudinal mode coupling occurs only with the nearest neighbour modes via the Slow varying LSHB been the fast carrier grating practically washed out by the diffusion process. The Slow-LSHB is on the contrary caused by the beating between co-propagating modes and it is the overlap of normal cosine functions with periods of few half-cavity length [32]. These papers have also shown the existence of a continuous power transfer from one mode to the other. The modes present periodic intensity fluctuations in the MHz range with an anti-phase dynamics that gives a compensation of the total power remaining practically constant with time [8], [32]. A similar behavior has been observed also for some QD lasers [33] where intensity fluctuations of the modes where measured with frequency of tens of MHz.

The goal of this work is the development of a Time Domain Traveling Wave (TDTW) model that can reproduce the experimental findings concerning the mode coupling and the SML in self assembled QD lasers. This is a complicate problem because the static behavior and the dynamics of the complex gain of QD active material need to be modeled including the inhomogeneous distributions of the QDs (i.e.: inhomogeneous gain broadening), the coupling among the different QDs via the homogeneous broadening linewidth and the fast gain recovery dynamics due to the carrier relaxation processes. An initial attempt in this direction was partially undertaken in [33] using a multi-population rate equation model. More recently a TDTW model capable of simulating SML in FP QD lasers was proposed in [34]; in that work the mechanism responsible for the mode coupling was completely attributed to a self-focusing Kerr effect modeled as an equivalent, lumped and ultra-fast SA included in the model at one facet of the device. Because of this instantaneous SA, stable pulses directly at the laser output facet were obviously obtained.

In this paper we address our attention to the simulation of QD FP lasers assuming that only carrier-photon interactions via mode beating, FWM and Fast- and Slow- LSHB due to the non-uniform carrier distribution are the most relevant phenomena in the laser structure we consider. We will show that the obtained simulation results are in line with the experimental results and can be used for a first interpretation of many of the experiments published in the literature.

II. Numerical model

In this paper we use an updated version of the TDTW approach we previously developed for the dynamical analysis of QD single mode semiconductor laser in [35] and we already presented in [36]; We report here only the most relevant equations for the model description. We make reference to [36] and [35] for the derivation of the model and to the Appendix, where we summarize the full rate equation system we use to model the carrier dynamics.

The spatio-temporal dynamics of the electric field along the FP cavity is described by the TW equations that for the slowly varying forward propagating electric field $E^{+}(z,t)$ is:

$$\begin{aligned}\frac{1}{v_{g0}}\frac{\partial E^{+}}{\partial t}+\frac{\partial E^{+}}{\partial z}=&-\left(\frac{\alpha_S}{2}+\mathrm{j}\beta_S\right)\left(S^{+}+2S^{-}\right)E^{+}\\&-\mathrm{j}\frac{\omega_0}{2\mathrm{c}\eta\varepsilon_0}\Gamma_{xy}P^{+}-\frac{\alpha_i}{2}E^{+}+S^{+}_{sp}\end{aligned}\tag{1}$$

The TW equation for the backward propagating component $E^{-}(z,t)$ can be obtained from (1) replacing the "+" superscripts with "−" and the plus sign on the LHS with a minus sign. In (1), ω_0 is the extracted reference frequency corresponding to a propagation constant β_0 such that the total electric field is:

$$\xi^{\pm}(t,x,y,z)=\phi(x,y)\left[E^{\pm}(z,t)\,\mathrm{e}^{-\mathrm{j}\omega_0 t}\mathrm{e}^{-\mathrm{j}\beta_0 z}+c.c.\right];\tag{2}$$

$\phi(x,y)$ is the transversal mode profile considered independent on (z,t). In (1) v_{g0} is the group velocity, η is the cold cavity effective refractive index, Γ_{xy} is the optical confinement factor; α_i is the waveguide loss and $S^{+}_{sp}(z,t)$ is the noise source due to spontaneous emission. The first term on the RHS accounts for the TPA contribution or Kerr effect modelled as an absorption and phase variation proportional (through the coefficients α_S and β_S) to the photon densities $S^{\pm}(z,t)=|E^{\pm}(z,t)|^2$ [37]; the factor of 2, appearing in the dependence with the photon densities, allows to account for the coupling between the forward and backward propagating field due to the standing wave pattern.

$P^{\pm}$ is the slowly varying component of the macroscopic polarization that accounts for the gain and refractive index dynamics; in the adiabatic approximation the macroscopic polarization is written as [36]:

$$\begin{aligned}&-\mathrm{j}\frac{\omega_0}{2\mathrm{c}\eta\varepsilon_0}\Gamma_{xy}P^{\pm}(z,t)=\\&\sum_{i=-N}^{N}\sum_{m=GS,ES}\widetilde{g}^{\pm}_{im}(z,t)\left(\rho^{e}_{im}(z,t)+\rho^{h}_{im}(z,t)-1\right)\cdot\\&\int_{-\infty}^{t}\Gamma\mathrm{e}^{\mathrm{j}\Delta\omega_{im}(t-\tau)}\mathrm{e}^{-\Gamma(t-\tau)}E^{\pm}(z,\tau)\,\mathrm{d}\tau\end{aligned}\tag{3}$$

where the first sum occurs over the $2N+1$ sub-groups we have used to represent the inhomogeneity of the QD ensamble. The second sum is over the ground state (GS) and the excited state (ES) where stimulated emission can take place. To represent

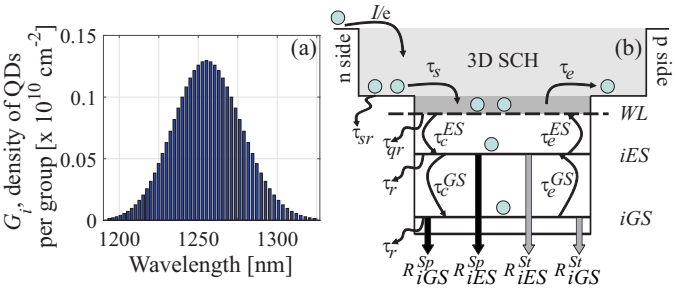

Fig. 1. (a) Sheet density of each QD sub-group (G_i) versus GS emission wavelength, here we consider $2N+1=51$ sub-groups. The index $i=0$ corresponds to the central group. (b) Schematic of the electron dynamics as it is considered in our model [35].

the inhomogeneous broadening of the gain, the QD ensemble is divided in several sub-groups, each with confined state recombination energy $E_{im} = \hbar(\omega_0 + \Delta\omega_{im})$. Assuming a Gaussian distribution of the QD size, the number of QDs per unit of area in each i-th group (G_i) is depicted in Fig. 1a.

On the right hand side of (3), the terms $\rho_{im}^{e,h}$ are the electron/hole occupation probability of the im confined state and $1/\Gamma$ is the dephasing time to account for the homogeneous broadening linewidth. The last term on the RHS of (3) represents the filtering of the electric fields $E^{\pm}$ to account for the complex gain wavelength dispersion. We define the filtered field as:

$$I_{im}^{\pm}(z,t) = \int_{-\infty}^{t} \Gamma \mathrm{e}^{\mathrm{j}\Delta\omega_{im}(t-\tau)} \mathrm{e}^{-\Gamma(t-\tau)} E^{\pm}(z,\tau)\,\mathrm{d}\tau. \quad (4)$$

In this work we assume that lasing occurs only from the GS whereas the modes at the ES wavelength always remain below threshold. Therefore the gain $\widetilde{g}_{im}^{\pm}(z,t)$ writes, for the GS, as:

$$\begin{aligned} \widetilde{g}_{iGS}^{+}(z,t) &= \frac{g_{0,iGS}}{1+\varepsilon\left(S_{iGS}^{+}(z,t)+2S_{iGS}^{-}(z,t)\right)} \\ \widetilde{g}_{iGS}^{-}(z,t) &= \frac{g_{0,iGS}}{1+\varepsilon\left(2S_{iGS}^{+}(z,t)+S_{iGS}^{-}(z,t)\right)} \end{aligned} \quad (5)$$

and for the ES as $\widetilde{g}_{iES}^{\pm}(z,t) = g_{0,iES}$, where

$$g_{0,iGS,ES} = \Gamma_{xy}\frac{G_i \mu_{GS,ES}|d_{GS,ES}|^2\omega_0}{2\mathrm{c}\eta\varepsilon_0\hbar\Gamma} \quad (6)$$

with $d_{GS,ES}$ the dipole matrix element of the GS and ES inter-band transition and $\mu_{GS,ES}$ the state degeneracy.

The expression in the denominator of (5) accounts for both self- and cross- compression of the GS gain [26] of the $i-$th QD population due to the photon densities $S_{iGS}^{\pm}$ resonant with that state; this photon density per unit volume reads as:

$$S_{iGS}^{\pm}(z,t) = 2\frac{\mathcal{R}\left\{E^{\pm *}(z,t)\, I_{iGS}^{\pm}(z,t)\right\}}{E_{im} w n_L h_{QD}} i = -N,\ldots,N \quad (7)$$

with w the waveguide width, n_L the number of QD layers and h_{QD} the thickness of a QD layer.

With the doubling of the backward/forward propagating photon densities in (5) we represent in an empirical way the effect (not otherwise included in our TDTW model) of the coupling between the backward and forward propagating field due to the carrier gratings caused by the electric field standing wave pattern with fast periodicity. We are aware that the present approach includes only empirically such mechanism; other models, as those in [8], [11], [38] applied up to now to the QW and QC laser case, account for this effect in a rigorous way. These models have not been implemented in our QD gain model for the difficulty of considering the effect of the standing wave patterns in all of the carrier states (GS, ES and WL) of all the $2N+1$ sub-groups of the QD ensemble used here to represent accurately the effects of the inhomogeneous gain broadening. Our approach aims indeed at a preliminary investigation of the QD laser mode dynamics that could be studied in future works adapting the previous models to the QD case. An expression similar to (5) could be considered however to account in our model also for other relevant non linear effects [39] not represented in rate equation approach.

Equations (1) to (7) are coupled with the rate equations describing the inter-sub band carrier dynamics for electrons and holes in the GS, ES, wetting layer (WL) and barrier states as sketched, for the electrons, in Fig. 1b. The full rate equation system is detailed in [35] and summarized in the Appendix of this paper. This set of equations is solved numerically with a finite difference algorithm, that is detailed in [36]; boundary conditions for the electric field are set at the FP facets that are considered as cleaved. The time step is $\delta t = 30\,\mathrm{fs}$ and $\delta z = v_{g0}\delta t$.

To conclude this Section, we summarize here the main characteristics intrinsically included in our model:

1) the inhomogeneous and homogenous broadening of the gain and effective refractive index spectrum,
2) the self-saturation of the complex gain of each QD group via the ε-parameter that account for the fast component of the standing wave pattern,
3) the spectral hole burning of electrons due to the finite relaxation time from ES1 to GS,
4) the coupling among the QDs via the common WL reservoir,
5) the hole dynamics (faster than electron dynamics) modelled with the approach presented in [35],
6) the spatial hole burning due to the slowly varying standing wave pattern; this pattern produces slowly varying carrier gratings that facilitate the coupling among co-propagating modes [32],
7) the FWM, the self-phase modulation and the cross-phase modulation due to carrier beating and spectral hole burning,
8) the effects due to TPA and Kerr lensing.

III. Simulation results

We consider a $1\,\mathrm{mm}$ QD Fabry-Perot laser operating at $1300\,\mathrm{nm}$; the material and device parameters are listed in Table I. The aim of this Section is showing how the gain compression plays a crucial role on the broadening of the optical spectrum and on the mode dynamics. In Section III.A we present the simulated static characteristics of the light out of the FP laser, in Section III.B we discuss the longitudinal mode dynamics

TABLE I
MAIN MODEL PARAMETERS

Symbol	Description	Values
	Material parameters	
η	Effective refractive index	3.34
n_L	Number of QD layers	15
N_D	QD surface density	$2.7 \times 10^{10}\,\mathrm{cm}^2$
N	Number of QD sub-groups	51
$\mu_{m,CB}$	CB states degeneracy $m = ES_1, GS$	4, 2
$\mu_{m,VB}$	VB states degeneracy $m = ES_4, \ldots, ES_1, GS$	6, 6, 6, 4, 2
$\hbar\Gamma$	Homogeneous linewidth	$10\,\mathrm{meV}$
ΔE_m	FWHM of the inhomogeneous gain broadening for $m = ES_1, GS$	45, $40\,\mathrm{meV}$
d_m	Dipole matrix element $m = ES_1, GS$	0.96, 0.6 e·nm
$\tau_c^{e,m}$	Electron relaxation times $m = WL, ES_1, GS$	3, 3, 1 ps
τ_{sp}^m	Spontaneous emission times $m = ES_1, GS$	1, 2 ns
α_i	Intrinsic waveguide losses	$5\,\mathrm{cm}^{-1}$
	Device parameters	
W	Ridge width	$5\,\mu\mathrm{m}$
L	Device length	$1\,\mathrm{mm}$
Γ_{xy}	Optical confinement factor	12 %
R_0, R_L	Terminal facets reflectivity	32 %

due to the coupling among the modes and in Section III.C we discuss the possibility of obtaining pulses out of the laser after the dispersion compensation in proper operation conditions.

A. Static characteristics

In this Section we analyze the numerical results of the simulation of the static characteristic of the laser in the current range from threshold to about 6 times the threshold current I_{th} and for different values of gain compression factor ε. This parameter was estimated to be in the range between $\varepsilon = 1.0 \times 10^{-16}\,\mathrm{cm}^3$ and $\varepsilon = 5.0 \times 10^{-15}\,\mathrm{cm}^3$ in [28]. In [30] a value of $\varepsilon = 1.0 \times 10^{-15}\,\mathrm{cm}^3$ was used to fit, using a numerical rate equation model, the small-signal modulation bandwidth measured for a QD FP laser similar to the one considered here.

Fig. 2 represents the calculated L-I characteristic normalized respect to the threshold current $I_{\mathrm{th}} = 60\,\mathrm{mA}$. Moderate values of gain compression (i.e.: $\varepsilon = 1.5 \times 10^{-16}\,\mathrm{cm}^3$) do not affect the linearity of the curve in the considered current range, whereas larger gain compression (i.e.: $\varepsilon = 1.5 \times 10^{-15}\,\mathrm{cm}^3$) also causes a non-linear increase of the power starting from a current about twice the threshold current. This strong saturation effect on the L-I characteristic is often mainly attributed to current leakage and temperature effects, which are not included in our model. We show here that a contribution to the non-linear L-I characteristic can be also associated to the broadening of the optical spectrum and the consequent involvement of lasing modes interacting with lateral QD groups (i.e.: $i = \pm 1, 2, 3$) respect to the central one (i.e.: $i = 0$). These groups, with smaller QD density G_i and larger detuning respect to the gain peak (see Fig. 1), need an higher carrier density (respect to the central one) to bring the lateral

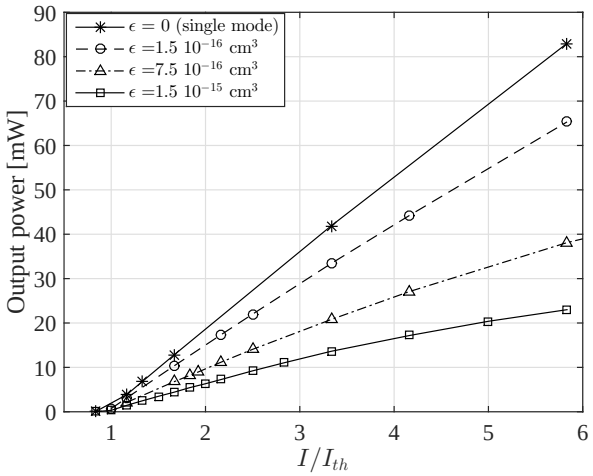

Fig. 2. Power versus current characteristic for different values of gain compression factor ε; $I_{\mathrm{th}} = 60\,\mathrm{mA}$.

modes of the spectrum to the lasing condition; therefore less carriers are available at the same pumping rate for photon emission.

The evolution of the optical output spectra as function of current and for the different values of ε is summarized in Fig. 3. The spectra were obtained simulating the laser switch-on with a current step at $t = 0$ and the electric field has been calculated from $t = 0$ to $t = 300\,\mathrm{ns}$ with a time step of $30\,\mathrm{fs}$. Due to the computational complexity of the considered model, one nanosecond of simulated time requires about 40 minutes of CPU time per $2.4\,\mathrm{GHz}$ XEON processor. The optical spectra have been obtained by the numerical Fourier transform of the electric field in the last $100\,\mathrm{ns}$ of the simulation; this corresponds to averaging over 4500 cavity round trips. In some cases longer simulation time would be necessary to assure that the power transfer among the modes (see Section III.B) reaches a stationary behavior but in any case a clear trend for the broading of the optical spectrum is demonstrated. Without gain compression the spectrum is practically single mode over all the considered current range (see top row of Fig. 3); increasing ε the spectrum starts single mode at threshold and then broadens increasing current (see mid row of Fig. 3). We have seen that this broadening is larger as ε increases. For example, for $\varepsilon = 1.5 \times 10^{-15}\,\mathrm{cm}^3$ in the bottom row of Fig. 3 the spectrum has a $-10\,\mathrm{dB}$ width of about $12\,\mathrm{nm}$ at only 1.7 times the threshold current. Increasing current the optical bandwidth gets larger but the spectrum shows two peaks, one at about $1245\,\mathrm{nm}$ and the other one at about $1265\,\mathrm{nm}$; the optical modes in the center (at about $1255\,\mathrm{nm}$) are suppressed of $9\,\mathrm{dB}$ at $4.2 I_{\mathrm{th}}$ and $5.8 I_{\mathrm{th}}$. This suppression of the modes in the center of the spectrum has been reported in several experimental works on QD lasers, for example in [29], [40], [41]. In Section III.B we will show that this is the consequence of the power transfer from the modes at the center of the spectrum to the modes at the border which can start lasing thanks to this photon injection.

The evolution of the $-10\,\mathrm{dB}$ optical bandwidth as function

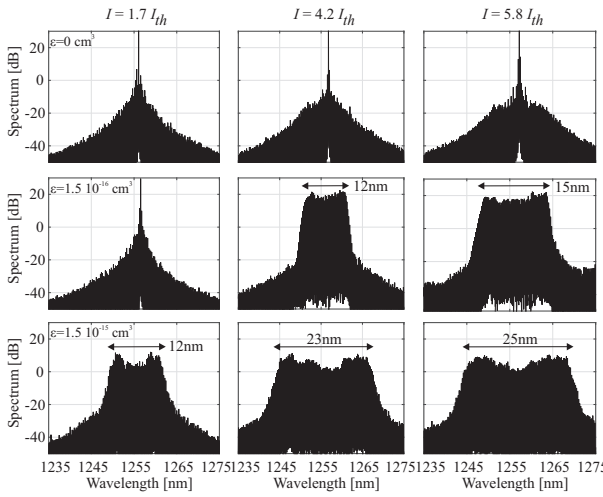

Fig. 3. Evolution of the optical spectra at the output facet of the FP lasers with increasing current above threshold: the top line is for $\varepsilon = 0$, the mid line for $\varepsilon = 1.5 \times 10^{-16}\,\mathrm{cm}^3$ and the bottom line for $\varepsilon = 1.5 \times 10^{-15}\,\mathrm{cm}^3$. The arrows evidence the $-10\,\mathrm{dB}$ optical bandwidth.

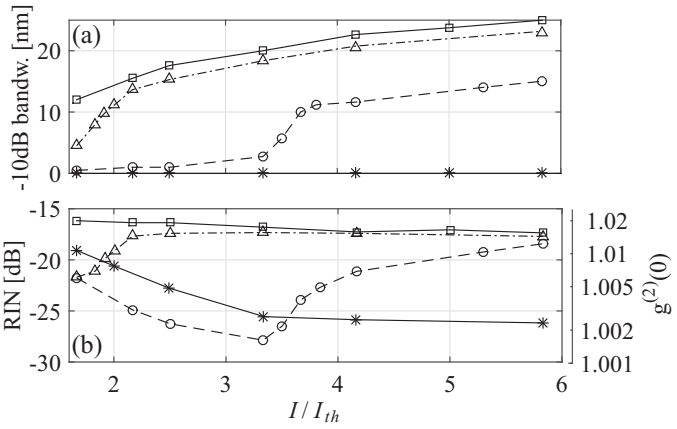

Fig. 4. (a) $-10\,\mathrm{dB}$ optical bandwidth and (b) RIN (on left axis) and $g^{(2)}(0)$ (on right axis) as function of the injected current above threshold for different values of gain compression factor ε; zero bandwidth in (a) means single mode. Legend is the same as in Fig. 2.

of current is plotted in Fig. 4a; similarly to the experimental results for QD and QDash lasers [13], [16] a clear spectral broadening with current is well reproduced by the simulations. The simulation results also point out that the sole inhomogeneous broadening of the gain spectrum is not sufficient to obtain a significant broadening of the optical spectrum; a strong non-linearity (only the selective self- saturation term of the GS gain of each QD sub-group by means of the photon density resonant with that state) is indeed sufficient for establishing the amplitude and phase coupling that makes possible the spectral broadening (see Section III.B).

In order to verify that the large spectra broadening can be attributed to the sole ε parameter and not to other effects such as the TPA and the Kerr, in the case $\varepsilon = 0$ we also investigated the role of the TPA and the Kerr effect. Using for TPA the values of the coefficients α_S and β_S generally reported in the literature (for example in [37]), no significant effects were obtained on the lasing spectra which remain single mode. For what concerns the Kerr effect, similarly to [11], we estimated, for the ridge waveguide structure considered in this analysis, the variation of the modal losses and of the mode confinement factor in the active region as function of the photon intensity. In our structure, differently respect to the QC case in [11], [12], the good field confinement in the low doping region makes the variation of the modal loss quite small with the photon density and therefore the Kerr effect in this structure cannot contribute significantly to the spectral broadening.

In the experiments a narrow RF line at the cavity free spectral range is considered a finger print of the phase locking of the modes; RF linewidth as narrow as $10\,\mathrm{kHz}$ have been reported for example in [19]. A correct estimation of such narrow linewidth would require averaging the laser output intensity over at least $500\,\mu\mathrm{s}$ which is a prohibitive computation time for our TDTW approach with our computational facilities. In this Section we will use the second-order coherence function ($g^{(2)}(\tau)$) as an estimation of a phase locking condition. We evaluate the second order coherence in $\tau = 0$ defined as:

$$g^{(2)}(0) = \frac{< I(t) \cdot I(t-\tau) >}{< I(t) >^2}|_{\tau=0} = 1 + \frac{\sigma_I^2}{I_0^2} \qquad (8)$$

where $I(t)$ is the intensity of the electric field:

$$I(t) = |E^+(z = L, t)|^2, \qquad (9)$$

I_0 is the average of $I(t)$ and σ_I^2 is the variance of the intensity. We note that the second term on the right hand side corresponds to the definition of the relative intensity noise ($RIN = \sigma_I^2/I_0^2$). In Fig. 4b we plot the RIN and the $g^{(2)}(0)$ calculated averaging over 4500 cavity round trips; for all the values of ε and currents considered, $g^{(2)}(0)$ is quite close to 1 and remains close to 1 even increasing current. This behavior resembles the case of a single mode laser [42] despite the very broad optical bandwidth of the spectrum. We use this result as indication of a phase locking condition among the modes. Indeed, in the case of a set of M uncorrelated modes the value $g^{(2)}(0)$ should get closer and closer to 2 as M increases; in [43] it is demonstrated that only 5-6 modes would be enough to approach the $g^{(2)}(0)$ value of a thermal source.

From Fig. 4b we observe that the case $\varepsilon = 1.5 \times 10^{-16}\,\mathrm{cm}^3$ gives the smallest RIN and $g^{(2)}(0)$ the closest to one. With increasing gain compression ($\varepsilon = 7.5 \times 10^{-16}\,\mathrm{cm}^3$ and $\varepsilon = 1.5 \times 10^{-15}\,\mathrm{cm}^3$) the RIN increases. We consider this increase as an indication of the fact that not all the modes in the very broad optical spectrum are phased locked. In particular we have observed that the modes with the highest power at the border of the optical spectrum give an incoherent contribution to the output electric field. At this respect, we compare in Fig. 5 the RF spectra calculated over 4500 cavity round trips for three different currents and ε values; the spectra have been shifted in frequency for better readability. Despite the fact that we cannot get a correct estimation of the RF linewidth, this analysis allows a qualitative comparison among the three cases: for $\varepsilon = 0$ there is no clear spectral line at cavity free spectral range. For $\varepsilon = 1.5 \times 10^{-16}\,\mathrm{cm}^3$ the lines are the narrowest, whereas they show a significant broadening for $\varepsilon = 1.5 \times 10^{-15}\,\mathrm{cm}^3$. The RF lines at $4.2 I_{\mathrm{th}}$ in Fig. 5b and at

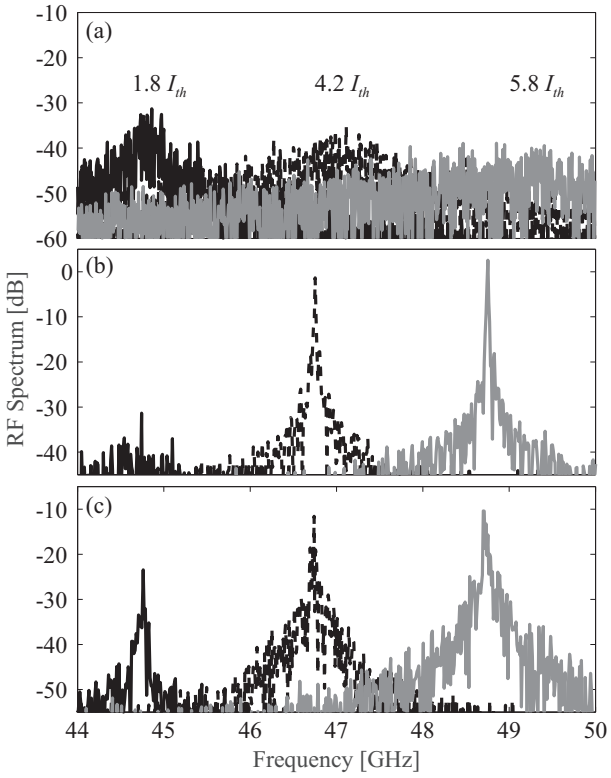

Fig. 5. RF spectra for injected currents of $1.7I_{\rm th}$, $4.2I_{\rm th}$, and $5.8I_{\rm th}$, with (a) $\varepsilon = 0$, (b) $\varepsilon = 1.5 \times 10^{-16}\,{\rm cm}^3$ and (c) $\varepsilon = 1.5 \times 10^{-15}\,{\rm cm}^3$. In all the cases the RF lines is at $46.74\,{\rm GHz}$; the RF spectra are shifted in the plot for a better comparison.

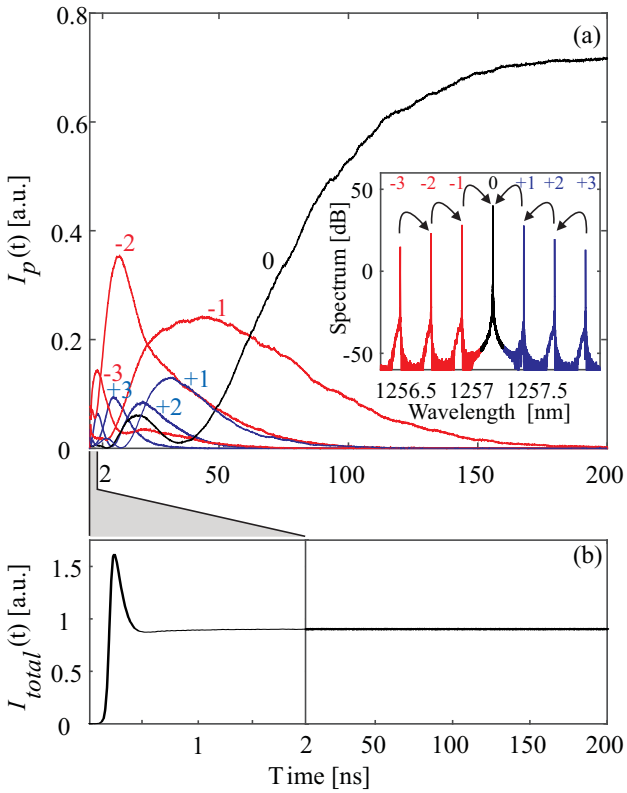

Fig. 6. (a) Intensity dynamics of the longitudinal modes shown in the inset and (b) sum of the intensity of all the lasing modes. The laser is switched on at $t = 0$ with a current step of $5.8I_{\rm th}$ and gain compression is $\varepsilon = 0\,{\rm cm}^3$.

$1.7I_{\rm th}$ in Fig. 5c corresponds both to an optical bandwidth of $12\,{\rm nm}$; however the line in Fig. 5b is smaller than the one in Fig. 5c as indicated also by the RIN in Fig. 4b. Our simulations also show that these noise features can be obtained only including, in the way it has been done, the gain self suppression term.

B. Longitudinal mode dynamics

To study the longitudinal mode dynamics we have filtered each line of the output optical spectrum with a narrow band-pass filter and then we have calculated its inverse Fourier transform; we obtain in this way the time evolution of the mode field $E_p(t)$, where p is the mode index. The mode intensity versus time of each longitudinal mode is given by $I_p(t) = |E_p(t)|^2$.

We investigate first the case $\varepsilon = 0$ at injection current equal to $5.8I_{\rm th}$. The resulting longitudinal mode dynamics is presented in Fig. 6a and the total intensity (i.e.: $I_{total} = \Sigma_p I_p(t)$) is in Fig. 6b. Fig. 6b shows that the relaxation oscillations (after the laser turn on at $t = 0$) are completely damped after $0.7\,{\rm ns}$ and the total intensity reaches a steady state at about $1.5\,{\rm ns}$. After $2\,{\rm ns}$ the total intensity is therefore constant and the power exchange among the various modes is only due to the mode coupling. We indeed observe that several modes (i.e.: $p = \pm 1, 2, 3, \ldots$) are present in the time range between 5 and $50\,{\rm ns}$. These modes are however not stable as they transfer their power towards the center of the spectrum (for example: $p = -3 \rightarrow -2$, $-2 \rightarrow -1$ and $-1 \rightarrow 0$); the central mode $p = 0$ collects all the power initially distributed over a broader optical spectrum and eventually the laser becomes single mode. This mode is the one closest to the gain peak of the central QD group $i = 0$.

To study the effect of a large ε on the longitudinal mode dynamics, we analyse in Fig. 7 the time evolution of the optical spectrum in the case $\varepsilon = 1.5 \times 10^{-15}\,{\rm cm}^3$ at current injection $2I_{\rm th}$; the optical spectrum reaches a steady state with a bandwidth of about $15\,{\rm nm}$. Due to the very broad spectrum the intensity dynamics ($I_p(t)$) of 60 longitudinal modes has been analyzed and the result is presented in Fig. 7a. The total intensity ($I_{total}(t)$ in Fig. 7b) reaches a constant steady state value at about $1\,{\rm ns}$ after the current switch-on with no relaxation oscillations as consequence of the high ε in line with the experiments in [29]. Despite the flat total power, the intensities of the lasing modes $I_p(t)$ present a very complicate dynamics. The optical spectrum starts rather narrow with the switch-on of 5-6 modes in the time range between $t = 0$ and $t = 10\,{\rm ns}$; due to the coupling among two adjacent co-propagating modes (made possible by the slowly varying spatial grating in the GS carriers) each of the modes transfer power to the two adjacent ones. Each mode, receiving the power, in turn transfers part of power back to the initial mode and part to the next one. This explains the almost regular pattern we observe in the wavelength region between the two

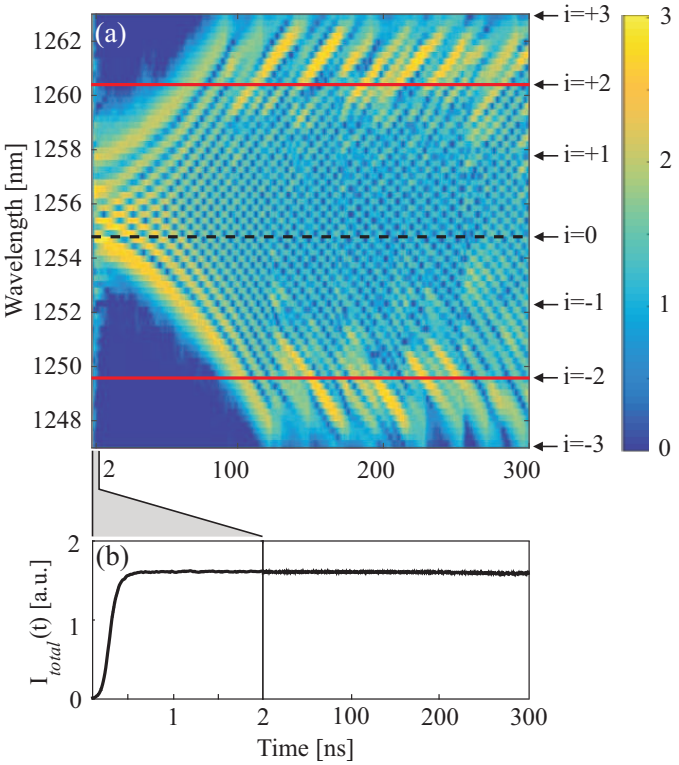

Fig. 7. (a) Map of the lasing longitudinal mode intensities vs time and (b) total power as sum of the intensity of all the lasing modes. The laser is switched on at $t = 0$ with a current step of $2I_{\rm th}$ and gain compression is $\varepsilon = 1.5 \times 10^{-15}\,{\rm cm}^3$. The indices i on the RHS of the map indicate the GS emission wavelength of the QD sub-groups involved in the lasing.

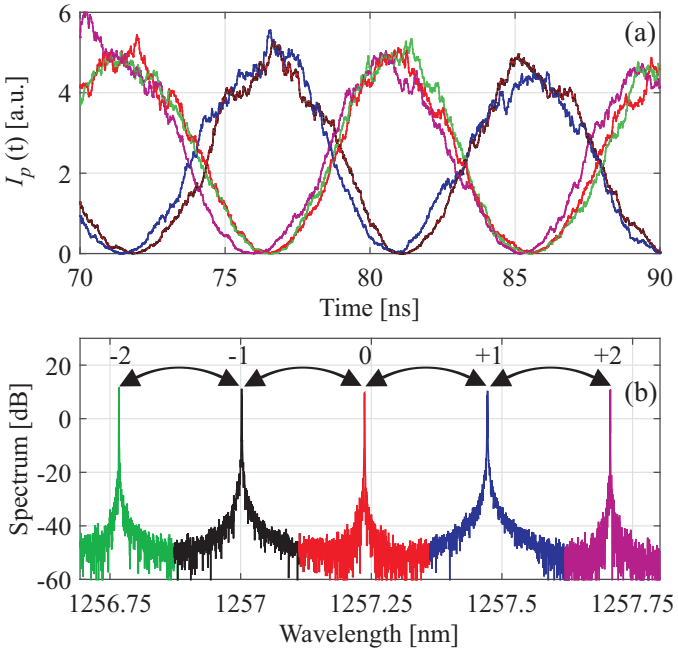

Fig. 8. (a) Intensity dynamics of 5 modes at the center of the optical spectrum considered in Fig. 7; (b) optical spectrum of the modes considered. Each line color in (a) corresponds to the colored spectral line in (b).

red lines in Fig. 7a. The dynamics of some of these modes in this spectral region is also plotted in Fig. 8. We see for example that the central mode $p = 0$ transfers power to the modes $p = \pm 1$; the mode $p = 1$ transfers power back to the mode $p = 0$ and to the mode $p = +2$. This continuous power transfer back and forth among the modes is indeed the physical mechanisms that guarantees an almost uniform distribution of the power among the lasing modes. We have also verified that, as soon as this coupling mechanism is established, the phases of the modes are locked (i.e.: each phase is almost constant with time with a constant phase difference between one mode and the other). The period of this intensity fluctuations is about $9\,{\rm ns}$ for the case shown in this figure. We have observed that the period gets smaller increasing current whereas it is longer reducing ε. For example for $\varepsilon = 1.5 \times 10^{-16}\,{\rm cm}^3$ and current $5.8I_{\rm th}$ it is about 70 ns. This result is in line with the experimental findings presented in [33].

The two red lines in Fig. 7a evidence the FWHM of the homogeneous broadening of GS emission of the central QD group ($i = 0$) whose recombination wavelength at $1254.8\,{\rm nm}$ is indicated by the dashed line. The power transfer from one mode to another also continues outside the red lines involving modes which are resonant with other QD groups such as the groups $i = \pm 2$. This power transfer produces a sort of optical injection mechanism which makes the modes, resonant with the QD groups $i = \pm 2$, turning on also if their gain is slightly smaller than the threshold gain. This may explain the higher mode intensities observed at the border of the spectrum. However, the strong power increase depletes the GS carriers and the gain causing after some time the switch-off of these lateral modes. They will switch-on another time when they will be feed again by enough power from the modes at the center of the spectrum. The continuous switch-on and off of the modes at the border of the spectrum causes incoherent fluctuations of the gain and refractive index all over the complex gain spectrum and may explain the increased RIN and the larger RF linewidth observed in Fig. 4b and Fig. 5c. Such incoherent contribution also causes instabilities on the pulses obtained after dispersion compensation. Applying a band pass filter at the laser output to cut off the modes outside the red lines, a train of pulses can be obtained directly at the laser output; such pulses are however rather unstable and show multiple peaks. From the analysis of the simulations results, we stress here the fact that the mode coupling induced by the large self saturation due to ε is the seeding mechanism for the spectral broadening and to start the pulse formation.

C. Phase locking and pulse formation

The measurements of the spectral phase using stepped heterodyne [44] or generalized multi-heterodyne [45] techniques is an important step in the characterization of a multi-mode FP laser. If the mode phases are constant in time and if they follow a parabolic profile versus the mode pulsation, then it is possible to compensate the corresponding Group Delay Dispersion (GDD) using a standard single mode fiber of suitable length in order to obtain a pulse train at the output of the system [10], [13], [46].

Here we present the numerical method implemented to evaluate the phase dynamics of each mode and, if locked, to

determine the optimal value of the GDD to introduce in the dispersion compensation algorithm. The aim is reproducing the generation of a pulse train after dispersion compensation as done in some experiments [10], [13], [46]. We assume that the electrical field associated to each longitudinal cavity mode can be written as $E_p(t) = \sqrt{I_p(t)}\mathrm{e}^{-\mathrm{j}(\omega_{0,p}t+\phi_p(t))}$, where $\phi_p(t)$ is the temporal variation of the phase respect to the reference mode wavelength $\omega_{0,p}$. With the same procedure used in Section III.B, we extract from the laser optical spectrum the mode fields $E_p(t)$. From the phase of the products $E_p(t)E^*_{p+1}(t)$ we define the time phase difference between two modes, $\Delta\phi_p(t)$, as:

$$\Delta\phi_p(t) = \angle E_p(t)E^*_{p+1}(t) - (\omega_{0,p} - \omega_{0,p+1})t \qquad (10)$$

and we calculate $\overline{\Delta\phi_p} =< \Delta\phi_p(t) >$. The standard deviation of $\Delta\phi_p(t)$ is evaluated to estimate the stability with time of the phase-locking.

The spectral phase profile, $\varphi(\omega_{0p})$, is evaluated as:

$$\varphi(\omega_{0p}) = \sum_{q=1}^{p} \overline{\Delta\phi_q} \qquad (11)$$

When the spectral phase profile follows an almost parabolic function the value of the GDD parameter is then extracted from the curvature of the parabola obtained fitting $\varphi(\omega_{0,p})$ in the least-squares sense. The dispersion compensation is simulated as a concentrated block with transfer function:

$$H_{comp}(\omega) = \mathrm{e}^{-\mathrm{j}\pi GDD\omega^2} \qquad (12)$$

and the final electric field after compensation is obtained as:

$$E_{comp}(t) = \mathcal{F}^{-1}\{\mathcal{F}\{E^+(z=L,t)\}H_{comp}(\omega)\}. \qquad (13)$$

From our simulations but also from the experimental results, it is possible to see that a proper compensation of the output power dispersion can be obtained in a wide range of parameters and currents; however stable mode locked pulses, suitable e.g. for optical communication applications, can been obtained only with moderate values of ε (e.g. equal or less than about $1.5 \times 10^{-16}\,\mathrm{cm}^3$ for our input parameter set) and not too high current injection (e.g. when the spectrum is not so broad to involve in the lasing also other QD groups outside the homogeneous broadening). We report here two examples of compensation applied to the device output field.

Fig. 9 presents the results of this analysis for the case $\varepsilon = 1.5 \times 10^{-16}\,\mathrm{cm}^3$ and injected current of $3.3I_{\mathrm{th}}$. The phase difference between couples of adjacent modes lying in the central part of the optical spectrum is practically constant with time, while modes at the border of the spectrum and with very low intensities have very large phase fluctuations. Fig. 9b shows a nice parabolic phase profile in line with [46]. The GDD extracted is $7.5\,\mathrm{ps}^2$. The output power obtained after the GDD compensation according to (13) is presented in Fig. 11a in dashed line and clearly exhibits pulses with a repetition rate of $44.9\,\mathrm{GHz}$ and a FWHM of $2.9\,\mathrm{ps}$. The pulse autocorrelation is reported Fig. 11b and it is compared with the autocorrelation of the laser output to show that the pulse formation is only due to the compensation algorithm.

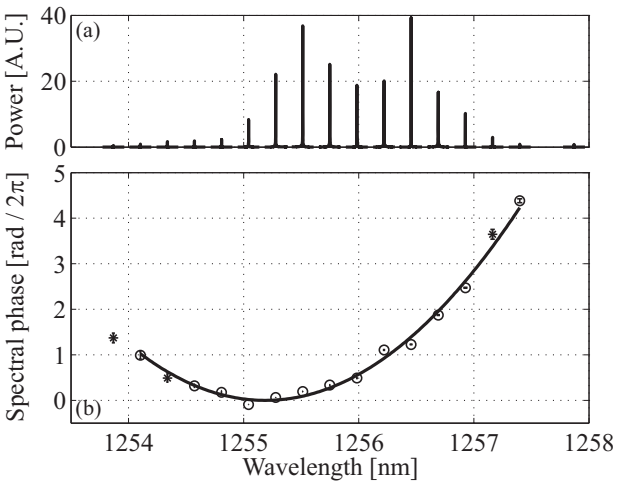

Fig. 9. (a) Optical spectrum and (b) spectral phase profile for the case $\varepsilon = 1.5 \times 10^{-16}\,\mathrm{cm}^3$ and injected current of $3.3I_{\mathrm{th}}$. The vertical bars quantify the standard deviation of $\Delta\phi_p(t)$ for each modes; the phases indicated with the circle/asterisks have standard deviation less/larger than $\pi/8$.

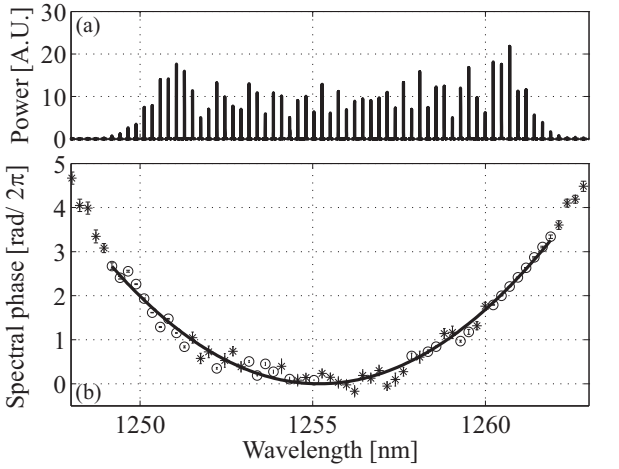

Fig. 10. Same as Fig. 9 for injected current $4.2I_{\mathrm{th}}$

Increasing the injection current, we expect shorter pulses as consequence of optical spectrum broadening shown in Fig. 3. We have analyzed the phase dynamics at current injection $4.2I_{\mathrm{th}}$ and the results are reported in Fig. 10. The corresponding GDD value is $0.6\,\mathrm{ps}^2$. This reduction of GDD with increasing current is in line with the measurements in [13]. The $44.7\,\mathrm{GHz}$ pulses obtained after the compensation are reported in Fig. 11a in solid line and have a $480\,\mathrm{fs}$ FWHM. The corresponding autocorrelation is in Fig. 11c. The pulses show however some instabilities that were not observed at $3.3I_{\mathrm{th}}$; this may be due to the modes evidenced with the asterisks in Fig. 9; these modes are not properly aligned with the parabolic profile and present large standard deviations.

IV. Conclusion

In this paper we have analyzed the longitudinal mode dynamics of a QD FP laser using the TDTW we developed in [35]. We have shown that we can reproduce the large

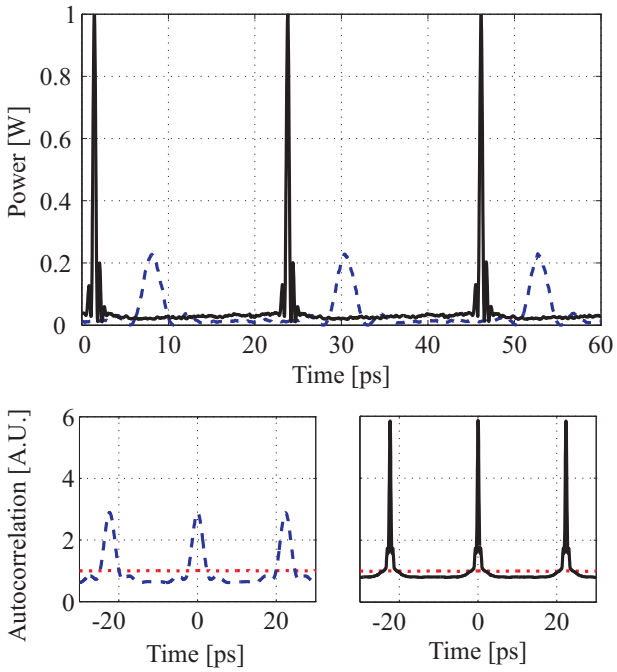

Fig. 11. (a) Pulse trains after the dispersion compensation and (b, c) corresponding autocorrelation functions. Dashed line is for the case in Fig. 9 and solid line for the case in Fig. 10; the red line in (b) and (c) is the autocorrelation calculated at the laser output before compensation.

broadening of the above threshold optical spectra as measured in experiments provided that we include in the model the self-gain compression factor parameter ε with values in the range between about $1 \times 10^{-16}\,\mathrm{cm}^3$ and $1 \times 10^{-15}\,\mathrm{cm}^3$. This range is considered quite typical for QD and QDash materials. This ε-parameter accounts in our model for the GS carrier grating (originated by the electric field standing wave pattern in the FP) that can not be washed out by carrier diffusion, being null in 0D states. Our simulation results have evidenced that the different self-gain saturation of the QD populations is the fundamental mechanism allowing to broaden the QD laser spectrum. The nonlinear interaction between the modes due to gain saturation establishes a continuous power transfer among the lasing modes allowing a wide optical bandwidth and almost equal power distributed among the modes. Analysing the intensity and phase dynamics of the modes, we have seen that in some cases the mode phases, when locked, have a parabolic distribution as a function of the mode frequency; such parabolic distribution can be compensated with propagation in a dispersive medium and pulses can be obtained in line with experimental results reported in the literature.

We have also found that, in the waveguide structure we have examined, other non-linearities such as TPA and Kerr effects produce a negligible enhancement of the optical bandwidth. Therefore we conclude that the very limited carrier diffusion and the fast GS gain recovery, typical of QDashes and QDs, are the mechanism seeding the coupling and the phase-locking among the modes.

V. Appendix

We summarize here the full set of the carrier rate equations we implemented to calculate the electron and hole occupation probabilities that appear in the polarization equation (3). This set of equations in also coupled with the TDTW equation of the electric field via the stimulated and spontaneous emission terms for the GS and ES.

For the electrons dynamics in conduction band we have:

$$\frac{\mathrm{d}\rho^e_{SCH}(z,t)}{\mathrm{d}t} = \frac{\eta_i J}{eD^e_{SCH}} + \frac{n_L D^e_{WL}}{D^e_{SCH}} \frac{\rho^e_{WL}}{\tau^{e,WL}_e}(1-\rho^e_{SCH}) - \frac{\rho^e_{SCH}}{\tau^{e,WL}_c}(1-\rho^e_{WL}) \tag{14}$$

$$\frac{\mathrm{d}\rho^e_{WL}(z,t)}{\mathrm{d}t} = \frac{D^e_{SCH}}{D^e_{WL} n_L} \frac{\rho^e_{SCH}}{\tau^{e,WL}_c}(1-\rho^e_{WL}) - \frac{\rho^e_{WL}}{\tau^{e,WL}_e}(1-\rho^e_{SCH}) + \sum_{i=-N}^{N}\left[-\frac{G_i}{N_D}\frac{\rho^e_{WL}}{\tau^{e,iES}_c}(1-\rho^e_{WL}) + \frac{G_i \mu_{ES}}{D^e_{WL}}\frac{\rho^e_{iES}}{\tau^{e,iES}_e}(1-\rho^e_{WL})\right] \tag{15}$$

$$\begin{aligned}\frac{\mathrm{d}\rho^e_{iES}(z,t)}{\mathrm{d}t} &= \frac{D^e_{WL}}{\mu_{ES} G_i}\frac{\rho^e_{WL}}{\tau^{e,iES}_c}(1-\rho^e_{iES}) \\ &- \frac{\rho^e_{iES}}{\tau^{e,iES}_e}(1-\rho^e_{WL}) - \frac{\rho^e_{iES}}{\tau^{e,GS}_c}(1-\rho^e_{iGS}) \\ &+ \frac{\mu_{GS}}{\mu_{ES}}\frac{\rho^e_{iGS}}{\tau^{e,GS}_e}(1-\rho^e_{iES}) - \frac{R^{Sp}_{iES}+R^{St}_{iES}}{\mu_{ES} n_L G_i}\end{aligned} \tag{16}$$

$$\begin{aligned}\frac{\mathrm{d}\rho^e_{iGS}(z,t)}{\mathrm{d}t} &= \frac{\mu_{ES}}{\mu_{GS}}\frac{\rho^e_{iES}}{\tau^{e,GS}_c}(1-\rho^e_{iGS}) \\ &- \frac{\rho^e_{iGS}}{\tau^{e,GS}_e}(1-\rho^e_{iES}) - \frac{R^{Sp}_{iGS}+R^{St}_{iGS}}{\mu_{GS} n_L G_i}\end{aligned} \tag{17}$$

where $\rho^e_{SCH,WL,ES,GS}$ are the electron occupation probabilities of the 3D SCH state, 2D WL state and the 0D GS and ES; η_i is the internal quantum efficiency, J is the current density, D^e_{SCH} is the SCH density of states per unit area; D^e_{WL} is the WL sheet density of state per QD layer, and N_D the density of QDs per layer. The carrier capture rate into one state occurs only via the carrier relaxing from the state immediately above and depends on the capture time constant $\tau^{e,SCH,WL,ES,GS}_c$, whereas the corresponding escape time $\tau^{e,SCH,WL,ES,GS}_c$ is calculated to assure the Fermi thermal equilibrium in absence of any excitation. R^{Sp}_{im} and R^{St}_{im} are the spontaneous emission and stimulated emission rate from the im-th state; for the stimulated emission rate per unit area we have:

$$\begin{aligned}&R^{St}_{im}(z,t) = \frac{2}{\hbar\omega_{im}}\left(\rho^e_{im}+\rho^h_{im}-1\right)\cdot \\ &\mathcal{R}\left\{\tilde{g}^+_{im}E^{+*}I^+_{im} + \tilde{g}^-_{im}E^{-*}I^-_{im}\right\} \\ &i=-N,\ldots,N \quad m=GS,ES\end{aligned} \tag{18}$$

while the spontaneous emission rate per unit area is

$$\begin{aligned}&R^{Sp}_{im}(z,t) = \frac{G_i \mu_m n_L \rho^e_{im}\rho^h_{im}}{\tau^{Sp}_m} \\ &i=-N,\ldots,N \quad m=GS,ES.\end{aligned} \tag{19}$$

For the hole rate equations we assume that the holes are always in quasi-thermal equilibrium within the confined states

and the WL and therefore, the hole distribution inside the QDs always follows a Fermi-Dirac distribution. With this assumption, the rate equations for the holes reduces to [35]:

$$\frac{\mathrm{d}\rho^h_{SCH}(z,t)}{\mathrm{d}t} = \frac{\eta_i J}{eD^h_{SCH}} + \frac{n_L N_D}{D^h_{SCH}} \frac{\rho^h_{QD}}{\tau_e^{h,QD}} \left(1-\rho^h_{SCH}\right) - \frac{\rho^h_{SCH}}{\tau_c^{h,QD}} \left(1-\rho^h_{QD}\right) \tag{20}$$

$$\frac{\mathrm{d}\rho^h_{QD}(z,t)}{\mathrm{d}t} = \frac{D^h_{SCH}}{n_L N_D} \frac{\rho^h_{SCH}}{\tau_c^{h,QD}} \left(1-\rho^h_{QD}\right) - \frac{\rho^h_{QD}}{\tau_e^{h,QD}} \left(1-\rho^h_{SCH}\right) - \sum_{i=-N}^{N} \sum_{m=ES,GS} \left[\frac{R^{St}_{im}}{n_L N_D} + \frac{R^{Sp}_{im}}{n_L N_D}\right] \tag{21}$$

where ρ^h_{SCH} is the hole occupation probability of the SCH state in valence band with density of state D^h_{SCH} and ρ^h_{QD} is the hole occupation probability of the hole QD state. Since this QD state is composed by the hole WL state and by the several hole 0D confined states, it is defined as:

$$\rho^h_{QD} = \sum_{m=GS,ES1,\ldots,ES4} \frac{\mu_m}{1+\mathrm{e}^{\frac{E^h_F - E^h_m}{KT}}} + \frac{D^h_{WL}}{N_D} \log\left(1+\mathrm{e}^{\frac{E^h_F - E^h_{WL}}{KT}}\right) \tag{22}$$

such that the sheet density of holes per QD layer is $N_D \rho^h_{QD}$. For the above set of hole equations D^h_{WL} is the hole density of states in the WL; E^h_F is quasi-Fermi level for the hole QD state, E^h_m are the energy levels for the hole 0D states and E^h_{WL} is the energy level of the WL; KT is the thermal energy.

ACKNOWLEDGMENT

The Authors acknowledge Dr. Stefan Breuer of Technical University of Darmstadt (Germany) for the interesting discussions on the interpretation of the experimental data and for the useful insight on the experimental techniques for the characterization of QD-ML lasers.

The Authors acknowledge also the Reviewers for the very useful comments and suggestions.

REFERENCES

[1] R. Graham and H. Haken, "Quantum theory of light propagation in a fluctuating laser-active medium," *Zeitschrift fr Physik*, vol. 213, no. 5, pp. 420–450, 1968. [Online]. Available: http://dx.doi.org/10.1007/BF01405384

[2] H. Risken and K. Nummedal, "Self-pulsing in lasers," *Journal of Applied Physics*, vol. 39, no. 10, pp. 4662–4672, 1968. [Online]. Available: http://scitation.aip.org/content/aip/journal/jap/39/10/10.1063/1.1655817

[3] L. Tiemeijer, P. Kuindersma, P. Thijs, and G. Rikken, "Passive fm locking in ingaasp semiconductor lasers," *Quantum Electronics, IEEE Journal of*, vol. 25, no. 6, pp. 1385–1392, Jun 1989.

[4] K. Shore and W. Yee, "Theory of self-locking fm operation in semiconductor lasers," *Optoelectronics, IEE Proceedings J*, vol. 138, no. 2, pp. 91–96, Apr 1991.

[5] M. Homar, J. Moloney, and M. San Miguel, "Travelling Wave Model of a Multimode Fabry-Perot Laser in Free Running and External Cavity Configurations," *Quantum Electronics, IEEE Journal of*, vol. 32, no. 3, pp. 553–566, Mar 1996.

[6] J. Renaudier, G.-H. Duan, P. Landais, and P. Gallion, "Phase Correlation and Linewidth Reduction of 40 GHz Self-Pulsation in Distributed Bragg Reflector Semiconductor Lasers," *Quantum Electronics, IEEE Journal of*, vol. 43, no. 2, pp. 147–156, Feb 2007.

[7] W. Yang, "Picosecond dynamics of semiconductor fabry perot lasers: A simplified model," *Selected Topics in Quantum Electronics, IEEE Journal of*, vol. 13, no. 5, pp. 1235–1241, Sept 2007.

[8] A. M. Yacomotti, L. Furfaro, X. Hachair, F. Pedaci, M. Giudici, J. Tredicce, J. Javaloyes, S. Balle, E. A. Viktorov, and P. Mandel, "Dynamics of multimode semiconductor lasers," *Phys. Rev. A*, vol. 69, p. 053816, May 2004. [Online]. Available: http://link.aps.org/doi/10.1103/PhysRevA.69.053816

[9] Y. Nomura, S. Ochi, N. Tomita, K. Akiyama, T. Isu, T. Takiguchi, and H. Higuchi, "Mode locking in Fabry-Perot semiconductor lasers," *Phys. Rev. A*, vol. 65, p. 043807, Mar 2002. [Online]. Available: http://link.aps.org/doi/10.1103/PhysRevA.65.043807

[10] K. Sato, "100 GHz optical pulse generation using Fabry-Perot laser under continuous wave operation," *Electronics Letters*, vol. 37, pp. 763–764(1), June 2001. [Online]. Available: http://digital-library.theiet.org/content/journals/10.1049/el_20010527

[11] A. Gordon, C. Y. Wang, L. Diehl, F. X. Kärtner, A. Belyanin, D. Bour, S. Corzine, G. Höfler, H. C. Liu, H. Schneider, T. Maier, M. Troccoli, J. Faist, and F. Capasso, "Multimode regimes in quantum cascade lasers: From coherent instabilities to spatial hole burning," *Phys. Rev. A*, vol. 77, p. 053804, May 2008. [Online]. Available: http://link.aps.org/doi/10.1103/PhysRevA.77.053804

[12] R. Paiella, F. Capasso, C. Gmachl, D. L. Sivco, J. N. Baillargeon, A. L. Hutchinson, A. Y. Cho, and H. C. Liu, "Self-mode-locking of quantum cascade lasers with giant ultrafast optical nonlinearities," *Science*, vol. 290, no. 5497, pp. 1739–1742, 2000. [Online]. Available: http://www.sciencemag.org/content/290/5497/1739.abstract

[13] R. Rosales, S. G. Murdoch, R. Watts, K. Merghem, A. Martinez, F. Lelarge, A. Accard, L. P. Barry, and A. Ramdane, "High performance mode locking characteristics of single section quantum dash lasers," *Opt. Express*, vol. 20, no. 8, pp. 8649–8657, Apr 2012. [Online]. Available: http://www.opticsexpress.org/abstract.cfm?URI=oe-20-8-8649

[14] K. Merghem, C. Calo, R. Rosales, X. Lafosse, G. Aubin, A. Martinez, F. Lelarge, and A. Ramdane, "Stability of Optical Frequency Comb Generated With InAs/InP Quantum-Dash-Based Passive Mode-Locked Lasers," *Quantum Electronics, IEEE Journal of*, vol. 50, no. 4, pp. 275–280, April 2014.

[15] Z. G. Lu, J. R. Liu, S. Raymond, P. J. Poole, P. J. Barrios, and D. Poitras, "312-fs pulse generation from a passive C-band InAs/InP quantum dot mode-locked laser," *Opt. Express*, vol. 16, no. 14, pp. 10 835–10 840, Jul 2008. [Online]. Available: http://www.opticsexpress.org/abstract.cfm?URI=oe-16-14-10835

[16] P. Poole, K. Kaminska, P. Barrios, Z. Lu, and J. Liu, "Growth of InAs/InP-based quantum dots for 1.55μm laser applications," *Journal of Crystal Growth*, vol. 311, no. 6, pp. 1482 – 1486, 2009. [Online]. Available: http://www.sciencedirect.com/science/article/pii/S0022024809001894

[17] R. Rosales, K. Merghem, C. Calo, G. Bouwmans, I. Krestnikov, A. Martinez, and A. Ramdane, "Optical pulse generation in single section InAs/GaAs quantum dot edge emitting lasers under continuous wave operation," *Applied Physics Letters*, vol. 101, no. 22, pp. –, 2012. [Online]. Available: http://scitation.aip.org/content/aip/journal/apl/101/22/10.1063/1.4768946

[18] T. Sadeev, D. Arsenijevic, D. Franke, J. Kreissl, H. Knzel, and D. Bimberg, "1.55-μm mode-locked quantum-dot lasers with 300 MHz frequency tuning range," *Applied Physics Letters*, vol. 106, no. 3, pp. –, 2015. [Online]. Available: http://scitation.aip.org/content/aip/journal/apl/106/3/10.1063/1.4906451

[19] M. Faugeron, F. Lelarge, M. Tran, Y. Robert, E. Vinet, A. Enard, J. Jacquet, and F. van Dijk, "High Peak Power, Narrow RF Linewidth Asymmetrical Cladding Quantum-Dash Mode-Locked Lasers," *Selected Topics in Quantum Electronics, IEEE Journal of*, vol. 19, no. 4, pp. 1 101 008–1 101 008, July 2013.

[20] M. Gaafar, D. A. Nakdali, C. Möller, K. A. Fedorova, M. Wichmann, M. K. Shakfa, F. Zhang, A. Rahimi-Iman, E. U. Rafailov, and M. Koch, "Self-mode-locked quantum-dot vertical-external-cavity surface-emitting laser," *Opt. Lett.*, vol. 39, no. 15, pp. 4623–4626, Aug 2014. [Online]. Available: http://ol.osa.org/abstract.cfm?URI=ol-39-15-4623

[21] G. L. Wojcik, D. Yin, A. R. Kovsh, A. E. Gubenko, I. L. Krestnikov, S. S. Mikhrin, D. A. Livshits, D. A. Fattal, M. Fiorentino, and R. G. Beausoleil, "A single comb laser source for short reach wdm

interconnects," vol. 7230, 2009, pp. 72 300M–72 300M–12. [Online]. Available: http://dx.doi.org/10.1117/12.816278

[22] R. Rosales, K. Merghem, A. Martinez, A. Akrout, J.-P. Tourrenc, A. Accard, F. Lelarge, and A. Ramdane, "InAs/InP Quantum-Dot Passively Mode-Locked Lasers for 1.55 μm Applications," *Selected Topics in Quantum Electronics, IEEE Journal of*, vol. 17, no. 5, pp. 1292–1301, Sept 2011.

[23] L. V. Asryan and R. A. Suris, "Longitudinal spatial hole burning in a quantum-dot laser," *Quantum Electronics, IEEE Journal of*, vol. 36, no. 10, pp. 1151–1160, Oct 2000.

[24] A. Capua, O. Karni, and G. Eisenstein, "A Finite-Difference Time-Domain Model for Quantum-Dot Lasers and Amplifiers in the Maxwell-schrödinger framework," *Selected Topics in Quantum Electronics, IEEE Journal of*, 2013.

[25] C. Su, "Dielectric grating induced by cavity standing wave as a new explanation of origin of nonlinear gain in semiconductor diode lasers," *Electronics Letters*, vol. 24, no. 7, pp. 370–371, Mar 1988.

[26] A. Mecozzi, A. D'Ottavi, and R. Hui, "Nearly degenerate four-wave mixing in distributed feedback semiconductor lasers operating above threshold," *Quantum Electronics, IEEE Journal of*, vol. 29, no. 6, pp. 1477–1487, Jun 1993.

[27] A. Pérez-Serrano, J. Javaloyes, and S. Balle, "Directional reversals and multimode dynamics in semiconductor ring lasers," *Phys. Rev. A*, vol. 89, p. 023818, Feb 2014. [Online]. Available: http://link.aps.org/doi/10.1103/PhysRevA.89.023818

[28] F. Grillot, B. Dagens, J. Provost, H. Su, and L. Lester, "Gain compression and above-threshold linewidth enhancement factor in 1.3-μm inas/gaas quantum-dot lasers," *Quantum Electronics, IEEE Journal of*, vol. 44, no. 10, pp. 946–951, Oct 2008.

[29] A. Capua, L. Rozenfeld, V. Mikhelashvili, G. Eisenstein, M. Kuntz, M. Laemmlin, and D. Bimberg, "Direct correlation between a highly damped modulation response and ultra low relative intensity noise in an inas/gaas quantum dot laser," *Opt. Express*, vol. 15, no. 9, pp. 5388–5393, Apr 2007. [Online]. Available: http://www.opticsexpress.org/abstract.cfm?URI=oe-15-9-5388

[30] D. Gready, G. Eisenstein, M. Gioannini, I. Montrosset, D. Arsenijevic, H. Schmeckebier, M. Stubenrauch, and D. Bimberg, "On the relationship between small and large signal modulation capabilities in highly nonlinear quantum dot lasers," *Applied Physics Letters*, vol. 102, no. 10, pp. –, 2013. [Online]. Available: http://scitation.aip.org/content/aip/journal/apl/102/10/10.1063/1.4795130

[31] A. E. Zhukov, M. V. Maximov, A. V. Savelyev, Y. M. Shernyakov, F. I. Zubov, V. V. Korenev, A. Martinez, A. Ramdane, J.-G. Provost, and D. A. Livshits, "Gain compression and its dependence on output power in quantum dot lasers," *Journal of Applied Physics*, vol. 113, no. 23, pp. –, 2013. [Online]. Available: http://scitation.aip.org/content/aip/journal/jap/113/23/10.1063/1.4811458

[32] D. Lenstra and M. Yousefi, "Rate-equation model for multi-mode semiconductor lasers with spatial hole burning," *Opt. Express*, vol. 22, no. 7, pp. 8143–8149, Apr 2014. [Online]. Available: http://www.opticsexpress.org/abstract.cfm?URI=oe-22-7-8143

[33] Y. Tanguy, J. Houlihan, G. Huyet, E. A. Viktorov, and P. Mandel, "Synchronization and clustering in a multimode quantum dot laser," *Phys. Rev. Lett.*, vol. 96, p. 053902, Feb 2006. [Online]. Available: http://link.aps.org/doi/10.1103/PhysRevLett.96.053902

[34] Z. Jiao, R. Zhang, X. Zhang, J. Liu, and Z. Lu, "Modeling of single-section quantum dot mode-locked lasers: Impact of group velocity dispersion and self phase modulation," *Quantum Electronics, IEEE Journal of*, vol. 49, no. 12, pp. 1008–1015, Dec 2013.

[35] M. Gioannini and M. Rossetti, "Time-domain traveling wave model of quantum dot dfb lasers," *Selected Topics in Quantum Electronics, IEEE Journal of*, vol. 17, no. 5, pp. 1318–1326, Sept 2011.

[36] M. Rossetti, P. Bardella, and I. Montrosset, "Modeling passive mode-locking in quantum dot lasers: A comparison between a finite-difference traveling-wave model and a delayed differential equation approach," *Quantum Electronics, IEEE Journal of*, vol. 47, no. 5, pp. 569–576, May 2011.

[37] D. Puris, C. Schmidt-Langhorst, K. Lüdge, N. Majer, E. Schöll, and K. Petermann, "Time-domain model of quantum-dot semiconductor optical amplifiers for wideband optical signals," *Opt. Express*, vol. 20, no. 24, pp. 27 265–27 282, Nov 2012. [Online]. Available: http://www.opticsexpress.org/abstract.cfm?URI=oe-20-24-27265

[38] J. Javaloyes and S. Balle, "Emission directionality of semiconductor ring lasers: A traveling-wave description," *Quantum Electronics, IEEE Journal of*, vol. 45, no. 5, pp. 431–438, May 2009.

[39] J. Huang and L. Casperson, "Gain and saturation in semiconductor lasers," *Optical and Quantum Electronics*, vol. 25, no. 6, pp. 369–390, 1993. [Online]. Available: http://dx.doi.org/10.1007/BF00420579

[40] S. G. Li, Q. Gong, Y. F. Lao, H. D. Yang, S. Gao, P. Chen, Y. G. Zhang, S. L. Feng, and H. L. Wang, "Two-color quantum dot laser with tunable wavelength gap," *Applied Physics Letters*, vol. 95, no. 25, pp. –, 2009. [Online]. Available: http://scitation.aip.org/content/aip/journal/apl/95/25/10.1063/1.3278594

[41] C. Mesaritakis, C. Simos, H. Simos, S. Mikroulis, I. Krestnikov, and D. Syvridis, "Pulse width narrowing due to dual ground state emission in quantum dot passively mode locked lasers," *Applied Physics Letters*, vol. 96, no. 21, pp. –, 2010. [Online]. Available: http://scitation.aip.org/content/aip/journal/apl/96/21/10.1063/1.3432076

[42] W. Chow, F. Jahnke, and C. Gies, "Searching for lasing threshold in a thresholdless laser," in *Semiconductor Laser Conference (ISLC), 2014 International*, Sept 2014, pp. 219–220.

[43] J. V. Goodman, *Statistical optics*. Wiley Edition, 2000.

[44] D. Reid, S. Murdoch, and L. Barry, "Stepped-heterodyne optical complex spectrum analyzer," *Optics express*, vol. 18, no. 19, pp. 19 724–19 731, 2010.

[45] A. Klee, J. Davila-Rodriguez, C. Williams, and P. J. Delfyett, "Characterization of Semiconductor-Based Optical Frequency Comb Sources Using Generalized Multiheterodyne Detection," *IEEE J. Sel. Top. Quantum Electron*, vol. 19, no. 4, p. 1100711, 2013.

[46] S. G. Murdoch, R. T. Watts, Y. Q. Xu, R. Maldonado-Basilio, J. Parra-Cetina, S. Latkowski, P. Landais, and L. P. Barry, "Spectral amplitude and phase measurement of a 40 ghz free-running quantum-dash modelocked laser diode," *Opt. Express*, vol. 19, no. 14, pp. 13 628–13 635, Jul 2011. [Online]. Available: http://www.opticsexpress.org/abstract.cfm?URI=oe-19-14-13628

Mariangela Gioannini received the Laurea degree in electronic engineering and the Ph.D. degree in electronic and communication engineering, both from Politecnico di Torino, Turin, Italy, in 1998 and 2002, respectively. She is currently Associate Professor with the Dipartimento di Elettronica e Telecomunicazioni, Politecnico di Torino. Her research interests include modeling of semiconductor lasers, amplifiers, and superluminescent light-emitting diodes based on quantum dot materials. Other topic of interest is the modelling and design of III-V solar cells. She has also been working on the design of widely tunable DBR and multi-section DFB lasers

Paolo Bardella received the Laurea degree in electronic engineering and the Ph.D. degree in electronic and communication engineering from the Politecnico di Torino, Turin, Italy, in 2001 and 2006, respectively. He is currently Assistant Professor with the Dipartimento di Elettronica e Telecomunicazioni, Politecnico di Torino, where he works on the simulation of multi-section semiconductor quantum dot lasers in mode-locking and self-pulsating regime. His current research interests also include the extension of the small and large signal modulation bandwidth of integrated semiconductor lasers.

Ivo Montrosset Ivo Montrosset (M92) was born in Aosta, Italy, in 1946. He received the Laurea degree in electronic engineering from the Politecnico di Torino, Turin, Italy, in 1971. From 1972 to 1986, he was with the Politecnico di Torino. In 1986 he was appointed Full Professor at the Universit di Genova, Genova, Italy. Since 1990, he has been Full Professor of optoelectronics at Politecnico di Torino. His main activities are in the field of guided wave-optics, solid-state and semiconductor lasers, and other related topics. Prof. Montrosset is a member of the IEEE Photonics Society.